VISIBLE-NEAR INFRARED MULTISPECTRAL IMAGING OF THE RAT DORSAL SKIN FLAP

Michael G. Sowa, Jeri R. Payette, Mark D. Hewko, and Henry H. Mantsch
Institute for Biodiagnostics, National Research Council Canada, Winnipeg, MB R3B 1Y6, Canada

ABSTRACT

Visible-near infrared multispectral reflectance image sets were acquired from the dorsal surface of rats both before and after elevation of reversed McFarlane skin flaps. Raw images were dominated by uneven surface illumination and shadowing along with the variation associated with instrument response. These interfering features obscured variation associated with a change in tissue reflectance, which is related to the degree of flap perfusion. Logarithmic residual preprocessing followed by principal component analysis of multispectral images could clearly detect a difference in the optical properties between the base and distal section of the flap. The difference in the reflectance properties correlates with the varying degree of tissue perfusion. Principal component analysis detected this optical difference between the well-perfused base of the skin flap and the compromised distal section of the flap immediately following surgery. The first visual signs of compromised tissue perfusion appeared only 6 or more hours after surgery. The results from this study indicate that the application of principal component analysis to discrete wavelength near infrared multispectral reflectance images of skin flaps can effectively distinguish reflectance changes related to the degree of tissue perfusion immediately following surgical elevation of the reversed McFarlane skin flap. © *1999 Society of Photo-Optical Instrumentation Engineers.* [S1083-3668(99)00104-5]

Keywords visible-near infrared spectroscopic imaging; principal component image analysis; skin flap perfusion.

1 INTRODUCTION

Adverse circulatory changes following the surgical elevation of a skin flap limits the supply of blood to the flap tissue. Regions of tissue that experience a prolonged and severe deprivation of blood supply will not survive. Early and reliable assessment of the degree of compromised tissue perfusion has important clinical implications for the ultimate survival of the skin flap. For centuries clinicians have empirically relied upon the visible appearance of tissue in the routine assessment of skin flap viability. Cyanosis and tissue swelling provide important clues as to the status of the flap. These symptoms cause the optical properties of well-perfused, healthy tissue and poorly perfused, compromised tissue to differ. Unfortunately, these differences only become clinically apparent several hours after surgery. This hampers early recognition of complications and hence delays steps that could be taken to intervene and alleviate the complication. Optical spectroscopy provides a nonsubjective means of classifying the changes in the optical properties of flap tissue which are characteristic of tissue compromise. Spectroscopic methods offer the promise of detecting and distinguishing these characteristic changes prior to the appearance of overt clinical signs of flap health or failure. Thus, spectroscopic analysis potentially enables earlier detection of perfusion related complications, thereby allowing prompt and effective intervention.

Near infrared[1–5] and visible spectroscopy[6–8] have been used to rapidly and noninvasively determine the regional tissue hemoglobin oxygen saturation at discrete locations of a skin flap. More recently we have extended this work to enable oxygenation and hydration imaging of the entire flap.[9,10] To date, univariate methods have largely been used in the analysis of skin flap spectroscopic or imaging data.[11] However, multivariate techniques show some promise in this application.[12,13] In general, multivariate analysis of multispectral images using principal component analysis (PCA) provides greater specificity and sensitivity over univariate models in a variety of remote sensing applications.[14–16] The variance partitioning provided by PCA of multispectral images also allows for data reduction and, at the same time, improves image signal-to-noise ratio. The primary goal of this paper is to determine the utility of PCA of visible-near infrared multispectral images of skin flaps.

This study uses the reverse McFarlane dorsal skin flap model[17] to demonstrate the potential of multispectral imaging utilizing both visible and near in-

Address all correspondence to M. G. Sowa. Tel: 204-984-5193; Fax: 204-984-5472; E-mail: mike.sowa@nrc.ca

frared wavelength measurement channels to detect poorly perfused tissues. Multispectral images of the rat dorsum were taken prior to and following surgical elevation of a skin flap. Logarithmic residual and optical density type preprocessing is used to help compensate for image artifacts arising from uneven surface illumination and the uneven surface topography of the rat dorsum as well as to correct for the instrument response function. PCA of the raw and preprocessed multispectral images are compared prior to surgery, in the early postoperative period and for up to 72 h following surgical elevation of the skin flap. The results demonstrate that PCA of visible-near infrared multispectral logarithmic residual corrected images and optical density images can reliably detect the reflectance variation along the length of the dorsal reversed McFarlane skin flaps that is related to the degree of tissue perfusion. This perfusion related change in the optical properties between the base and distal sections of the skin flap can be detected by the PCA analysis immediately following elevation of the flap. Visual clues about the status of these regions of tissue require 6 h or more to manifest. The distinct difference in reflectance between the base and distal ends of the flap corresponds to the expected blood supply for the described model and also correlates with laser Doppler blood flow measurements made along the length of the flap.

2 METHODS AND MATERIALS

2.1 ANESTHESIA AND SURGICAL PROCEDURE

All experiments conformed to the guidelines set out by the Canadian Council on Animal Care regarding the care and use of experimental animals and were approved by the Animal Care Committee of the National Research Council of Canada.

This study was done on 3 by 10 cm reverse McFarlane flaps raised on the dorsum of 13 Sprague Dawley rats weighing between 380 and 410 g. Twenty min prior to surgery, the rats were premedicated with 0.05 mg/kg atropine sulfate administered subcutaneously in the ventral abdomen. The rats were then anesthetized (1.2%–2% isoflurane inhalation anesthesia) and placed on a circulating water blanket in order to maintain body temperature at $37 \pm 0.5 °C$ during surgery. Once body temperature was stable, pre-elevation multispectral images, spectra, and laser Doppler measurements were acquired. Figure 1(A) illustrates the dorsal reversed McFarlane skin flap model used in the present study and the sites at which spectra and laser Doppler measurements were made. In this model, three sides of the flap are incised and elevated while one end of the skin flap, termed the vascular pedicle or base, is left attached to the remaining skin. Sacral vessels, which are contained within the pedicle and which run along the length of the flap, are left intact
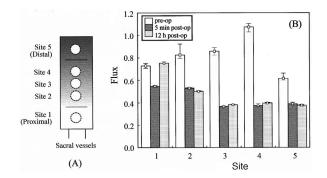

Fig. 1 (A) Schematic illustration of the dorsal reversed McFarlane skin flap model in the rat. (B) Laser Doppler flux measurements of blood flow at discrete sites along the dorsum of the rat. Preoperative measurements are compared to laser Doppler flux measurement taken 5 min and 12 h after surgical elevation of the skin flap.

and become the primary blood supply for the entire flap. A 3 cm wide by 10 cm long flap consisting of skin and underlying panniculus carnosus based on the sacral vessels was raised and the underlying wound was sutured closed. The flap was then repositioned over the closed wound and held in place with sutures. The surgery was done under aseptic techniques and an antibiotic ointment (Furacin) was applied around the flap edges and along the sutures of the closed wound. Postoperative analgesia was provided by subcutaneous injection of Buprenorphine (25 μg/kg) every 8 h for the remaining duration of the experiment. Postelevation multispectral images, visible-near infrared spectra, and laser Doppler measurements were acquired immediately upon completion of the surgical procedure as well as at 1, 2, 6, 12, 24, and 48 h following surgery. After a 72 h postoperative observation period, a final visual assessment of the flap was made, after which the rat was sacrificed.

2.2 MULTISPECTRAL IMAGING AND SPECTROSCOPY

Two multispectral image data sets were acquired. Visible-near infrared reflectance images of 256 $\times$ 256 pixels were collected at 430, 550, 565, 760, 830, and 980 nm using a series of 10 nm full width half height (FWHH) bandpass filters (OCLI, Santa Rosa, CA) positioned in front of a Nikon Macro AF60 lens mounted on a Photometrics Series 200 (Photometrics, Tuscon, AZ) charge coupled device (CCD) camera. Near infrared multispectral images (650, 700, 760, 800, 850, 900, and 980 nm) were collected with a 10 nm bandpass (FWHH) liquid crystal tunable filter (Cambridge Research Instruments, Cambridge, MA) mounted on a Nikon Macro lens fitted on a back illuminated CCD camera (Princeton Instruments, Inc., Trenton, NJ). Laser Doppler measurements and visible-near infrared spectra were collected at five discrete locations along the rat dorsum [see Figure 1(A)]. Visible-near infrared spectra were collected with an NIR Systems 6500 spectrom-

eter (Foss, Silver Springs, MA) using a custom bifurcated fiber optic bundle (Fiberguide Industries, Stirling, NJ). A 99% Spectralon® reflectance standard (LabSphere, Inc., North Sutton, NH) was used as a reference to convert raw data into reflectance spectra. Each reflectance spectrum consisted of 32 coadded scans collected between 400 and 1100 nm at 10 nm resolution. Laser Doppler blood flow measurements were recorded as the mean of 30 readings collected at 1 s intervals using a floLAB laser Doppler monitor (Moor Instruments Inc., Wilmington, DE).

Multispectral images, near infrared spectra, and laser Doppler measurements were acquired prior to surgery and immediately following surgical elevation of the flap as well as at 1, 2, 6, 12, 24, and 48 h following surgery. The visible-near infrared multispectral data set was acquired on four flaps while the near infrared image set was repeated on six flaps. In a further series of three flaps, vascular clamps were applied to the base of the skin flap 1 h following surgery and left in place for an additional 1 h. Near infrared imaging data were collected prior to vascular clamping, during the application of the clamps, and for up to 3 h following release of the clamps.

2.3 MULTISPECTRAL IMAGE PROCESSING

Raw multispectral images contain information on the spectral and spatial response function of the instrumentation as well as the sample. Generally, it is the spectral–spatial response of the sample that is of interest and not the instrument response function. Thus, a means of eliminating the instrument response profile in the multispectral image set is desirable. This is usually accomplished by taking the ratio of the sample images (S) with respect to a reference multispectral image (R). The reference material is of known and preferably constant reflectance across the spectral range of interest. In optical density reflectance images, $X = \log R - \log S$, the reference material provides a measure of the instrument response function and therefore the method effectively ratios out the instrument response function from the resultant optical density image set X. However, the method cannot compensate for artifacts arising from sample topology leading to shadowing or situations where surface illumination changed between the time the reference images and the sample images were acquired. Clinically, especially during surgery, such situations arise frequently.

The logarithmic residual method[15] was developed for remote sensing situations where a reference image set was not available and where the illumination and surface topography were not constant. The measured raw multispectral image of the sample S_{ij} (where i = pixel number and j = wavelength channel number) is assumed to be the

$$S_{ij} = T_i X_{ij} I_j \tag{1}$$

product of the wavelength response of the system I_j with a topographical factor related to the spatial portion of the instrument response function, unevenness of the surface illumination and surface topography of the rat dorsum T_i, and the tissue reflectance X_{ij}. Approximate optical density reflectance images can be obtained using the logarithmic residual method which ratios estimated topographical and illumination factors from the measured images. The logarithmic residual method effectively mean centers the multispectral data set over both the image pixel and wavelength channel dimensions and adds the grand mean back to the resultant image following a log transformation of the sample images,

$$\tilde{X}_{ij} = \frac{1}{M} \sum_i \ \log S_{ij} + \frac{1}{N} \sum_j \ \log S_{ij} - \log S_{ij}$$

$$- \frac{1}{NM} \sum_{i,j} \ \log S_{ij}, \tag{2}$$

where N is the total number of pixels and M is the number of wavelength channels. While attempting to compensate for surface and illumination dependant artifacts present in the multispectral image, the logarithmic residual method has the added advantage that a reference multispectral image set is not required. However, in our experience, the logarithmic residual method usually compensates inadequately for the response of the instrument. When a reference reflectance image set is available, a preferable approach is to use the reference image set to correct primarily for the wavelength dependence of the instrument response and the mean or median sample image to correct for illumination and sample dependant artifacts:

$$\tilde{X}_{ij} = \frac{1}{M} \sum_i \ \log R_{ij} + \frac{1}{N} \sum_j \ \log S_{ij} - \log S_{ij}$$

$$- \frac{1}{NM} \sum_{i,j} \ \log S_{ij}. \tag{3}$$

PCA was carried out on raw, optical density, and logarithmic residual preprocessed multispectral images. PCA is a diagnostic method aimed at determining generalized components of variance in the data set. Prior to a principal component (PC) decomposition, the multispectral image sequence was scaled to unity variance at each wavelength channel. This corresponds to performing PCA on the correlation matrices of the multispectral image sequence. Singular value decomposition[18] decomposes the multispectral reflectance image X into a set of eigenvectors U and V, where V^t indicates transpose of V

$$X = U a^{1/2} V^t, \tag{4}$$

which diagonalize the cross product matrices XX^t and X^tX, respectively, and are associated with the common set of eigenvalues a. The eigenvector basis V spans the wavelength channel (column) space thus providing the principal component loadings for the wavelength channels (variables). The eigenvector basis U spans the image pixel (row) space of the original data matrix S and corresponds to the principal component scores for the images (objects).

In the multispectral images, the number of image pixels ($N=65536$) greatly exceeded the number of wavelength channels ($M=6$ or 7). Thus, the eigenvectors V (principal component wavelength loadings) of the smaller dimensional $M \times M$ space of X^tX were first calculated and used with the original data matrix X in conjunction with Eq. (4) to reconstruct the image principal component scores U (score images). The kth normalized eigenvalue provides a measure of the percent variance accounted for by the kth principal component of the expansion of the multispectral image matrix. Thus, the ordered set of principal components accounts for successively smaller fractions of the variation in the tissue reflectance.

Following the image preprocessing steps described above, the first principal component on average accounted for 75.5% of the variation in the data set. The first three components accounted for more than 93% of the variance in the data and were retained while the higher order components, accounting for less than 7% of the variance, were discarded in any further analysis.

3 RESULTS AND DISCUSSION

Figure 2 shows the visible-near infrared absorption spectra of hemoglobin (Hb), oxyhemoglobin (HbO$_2$), and water (H$_2$O), as well as some of the wavelength channels used in the multispectral image sequences. The wavelength channels selected for the multispectral image sets correspond closely to absorption band maxima or isobestic points for Hb, HbO$_2$, or H$_2$O.[19,20] The 430, 565, and 760 nm channels closely correspond to absorption maxima of Hb. The 430 nm channel is centered just on the long wavelength side of Hb Soret (B band) absorption band maximum and encompasses only the long wavelength tail of the HbO$_2$ Soret band. The 565 nm channel lies between the Q_v and Q_o absorption bands of HbO$_2$, at a point of minimum absorption for HbO$_2$, but centered on the shoulder of the Q_v absorption maximum of Hb. The wavelength channels at 650 and 700 nm exploit the large differential absorption between Hb and HbO$_2$, while the 760 nm imaging channel is centered on the III charge transfer band of Hb. Thus these series of wavelengths were selected because of their sensitivity to changing hemoglobin oxygenation. Conversely, the 550 and 800 nm channels are near Hb/HbO$_2$ isobestic points (where Hb and HbO$_2$ ab-
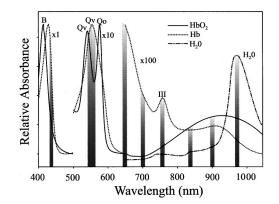

Fig. 2 Absorption spectra in the spectral region 400–1080 nm of hemoglobin (Hb), oxyhemoglobin (HbO$_2$), and water (H$_2$O). The multispectral imaging channels centered at 430, 550, 565, 650, 700, 760, 830, 900, and 980 nm are shown as shaded bars and are ± 5 nm wide. The Soret band and the vibronic transition band maxima of Hb and HbO$_2$ are labeled as B and Q_o (Q_v), respectively. The distinct charge transfer band of Hb is signified with a III label while the second overtone region of water is labeled as H$_2$O.

sorb equally) and are relatively insensitive to varying hemoglobin oxygenation. The 550 nm channel is centered on the Hb/HbO$_2$ isobestic point where the Q_v vibronic transitions for these biomolecules cross over. The 800 and 830 nm channels encompass the isobestic region of the Hb–HbO$_2$ III charge transfer bands. The 850 and 900 nm channels sample the III charge transfer band maximum of HbO$_2$. This region has little underlying absorption from Hb. The 980 nm channel was chosen in the multispectral imaging sequences to provide water related information. This wavelength channel is centered on the second OH stretching overtone region of H$_2$O.

Spatial variation in tissue blood volume results in a corresponding variation in the tissue reflectance at the wavelengths where Hb, HbO$_2$, and H$_2$O have a significant absorption. Spatial variation in hemoglobin oxygen saturation results in a change in the differential reflectance at absorption wavelengths associated with HbO$_2$ relative to wavelengths where Hb preferentially absorbs. However, reflectance intensity at isobestic wavelengths are unaffected by spatially varying oxygen saturation when blood volume remains constant. Changes which are observed at the 980 nm water absorption band but which do not correlate with observations at the Hb/HbO$_2$ isobestic reflectance wavelength arise from changes in tissue hydration, which are independent of blood volume changes. Images based on carefully selected visible and near infrared wavelengths should potentially be able to provide information on blood volume or total hemoglobin, the fraction of oxygenated hemoglobin, and the relative degree of tissue hydration.

Figure 1(A) indicates the five discrete sites at which laser Doppler and full range (400–1100 nm) spectroscopic measurements were taken. The re-
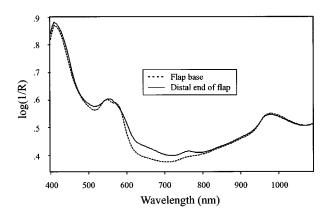
Fig. 3 Reflectance spectra of the rat dorsal skin flap taken immediately following surgical elevation of the flap from near the vascular base of the skin flap (dashed trace-site 1) and from near the distal end of the skin flap (solid trace-site 5).

Fig. 4 Selected gray-scale reflectance images of a flap acquired 1 h after surgery, 650 (A), 760 (B), 830 (C), and 980 nm (D).

verse McFarlane flap is a pedicle flap model and derives its blood supply from sacral vessels at the base or pedicle of the flap. Therefore the base of the skin flap, proximal to the blood supply, is well perfused while the distal end (which is far removed from the blood supply) is poorly perfused. Any blood flowing to the distal end of the flap should also be poorly oxygenated. Figure 1(B) compares laser Doppler blood flow measurements made along the length of the rat dorsum prior to surgery, immediately following surgical elevation of the flap and 12 h following surgery. Laser Doppler flux measurements indicate an instantaneous drop in perfusion along the entire length of flap immediately upon surgical elevation. This immediate drop in flow is most pronounced in the distal half of the flap and is consistent with the pedicle nature of the skin flap. Blood flow re-establishes to preoperative levels at the proximal site (site 1) within 12 h of surgery. Blood flow just proximal to the flaps midline (site 2) remains depressed even 12 h after surgery. However, the measured flow at site 2 is significantly higher than that measured at sites in the distal half of the skin flap. Laser Doppler measurements indicate a decrease in blood flow and blood volume from the proximal to the distal end of the flap. Total hemoglobin, the fraction of oxygenated hemoglobin, and water content are also expected to decrease along the length of the flap.

Figure 3 compares the visible-near infrared reflectance spectrum from the base [site 1, see Figure 1(A)] and the distal end [site 5, see Figure 1(A)] of the flap immediately following surgical elevation of the skin flap. Note that reflectance spectra are plotted in the usual log(reference/sample), optical density scale. The solid trace spectrum is taken near the distal end of the flap (site 5) while the dashed spectrum arises from near the base of the flap (site 1).

Examination of the visible images acquired in the early postoperative period reveal little or no difference in the reflectance of the tissue along the length of the pedicled skin flap. The 550 nm channel might
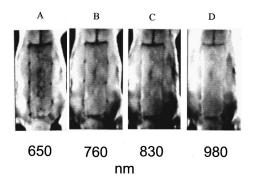
be expected to be sensitive to overall blood volume changes since both Hb and HbO_2 contribute equally to the tissue absorption at this wavelength while the 430 and 565 nm channels might be expected to distinguish regions of varying tissue hemoglobin oxygen saturation. However, the 430, 550, and 565 nm channel images are highly correlated ($r > 0.85$) and essentially provide redundant image information. These visible image channels are also influenced by interfering skin pigmentation absorptions, such as melanin, which further complicates visible spectroscopy-based approaches of assessing skin flap tissue viability. The high degree of overlap between the Hb and HbO_2 absorptions in the visible region (see Figure 2) gives rise to the high correlation between the visible wavelength channels. The spectra presented in Figure 3 reveal only subtle differences between the spectra from the base and distal end of the skin flap in the visible region. Thus, based on the spectra, one can rationalize why little or no reliable clinical information can be derived from a cursory examination of visible images or spectra. Likewise, the long wavelength region of the spectrum shows no difference between skin flap sites and the image channels >800 nm display no contrast along the length of the flap.

Based on the spectra in Figure 3, the most promising region for optical discrimination between the base and distal ends of the flap lies in the 650–800 nm region. Images in this red visible-near infrared region should provide the best contrast along the length of the flap. The 800 nm region which is near an Hb/HbO_2 isobestic point was expected to be sensitive to blood-volume variations, but individual images display near equal reflectance from the base and distal zones of the flap. Likewise the 650, 700, and 760 nm images provide no significant contrast along the length of the flap. This is evident in Figure 4 in which the raw near infrared flap images are presented.

Cursory analysis of the raw, optical density and logarithmic residual corrected multispectral images collected in the early postoperative period did not reveal a significant difference in the reflectance properties between the well perfused base of the
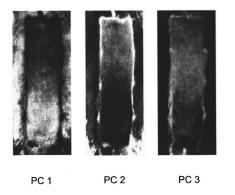
Fig. 5 Gray-scale principal component score images based on near infrared multispectral reflectance images of a flap acquired 1 h after surgery, first (A), second (B), and third (C) principal component score images.

flap and the poorly perfused distal section of the flap (see Figure 4). It is not until about 12 h following surgery when the optical properties between the proximal and distal ends of the flap are sufficiently different so that the contrast along the length of the flap can be distinguished in the individual images. However, visually at 12 h, signs of distal end necrosis generally become apparent. Thus analysis of raw and optical density single wavelength visible and near infrared images provides no significant advantage over standard visual assessment of the tissue.

PCA decomposes the multispectral image sequence into a set of uncorrelated PCs which partition the variance within the data set into its independent, rank ordered, sources. The high degree of correlation between the wavelength channels also suggests that a truncated PC expansion could effectively provide the relevant tissue perfusion information in a more compact and significantly higher signal-to-noise representation. PCA of the raw multispectral image data is generally not satisfactory for the near infrared or the visible-near infrared data sets. In the raw multispectral images the instrument response function, illumination, and shadowing artifacts dominate the variation observed in the data set, which causes features to appear in the first few PCs. However, transforming the raw data into optical density images and logarithmic residual corrected images drastically reduces instrument response and image artifact contributions to the variance. For example, the first three PC score images derived from a logarithmic residual corrected near infrared multispectral image data set, acquired 1 h after skin flap surgery, are reported in Figure 5. These three PCs account for 93% of the variation in the data set with PCs 1 and 2 displaying a distinct gradient in score values along the length of the flap and PC 3 displaying high score values in the center portion of the flap.

The first PC score images derived from the logarithmic residual corrected near infrared multispec-
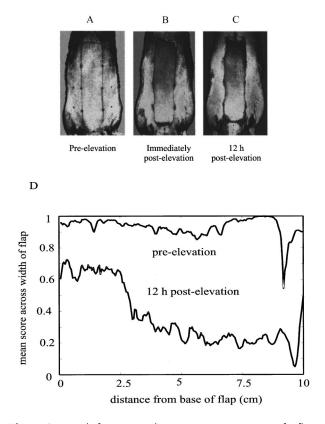

Fig. 6 Gray-scale first principal component score images of a flap derived from logarithmic residual corrected near infrared multispectral images, preop (A), as well as 5 min and 12 h after surgery (B), (C). Panel (D) compares the mean of the first PC score across the width of the flap as a function of distance from the base of the skin flap for the pre-elevation and 12 h postsurgery time points. The PC scores over all three flap images were normalized between 0 and 1 to compensate for scale dependent changes between measurement time points.

tral images acquired preoperatively, immediately following surgical elevation of the skin flap, and 12 h after surgery are compared in Figure 6. These PC score images correspond to the same flap on which the laser Doppler measurements are summarized in Figure 1(B). The PC images acquired prior to surgery [Figure 6(A)] display uniform scores over the rat dorsum. Thus there is little variation in the tissue reflectance over the rat dorsum before surgery. Immediately after surgery [Figures 5 and 6(B)] the first PC score image displays a distinct gradient along the length of the skin flap. This gradient persists in the first PC score images acquired at later times, up to 12 h, following surgery [see Figure 6(C)]. In Figure 4(D) the average of the first PC score across the width of the flap is plotted as a function of distance from the base of the skin flap. The proximal end of the flap near the base of the flap and the uninvolved dorsal tissue as well as the full dorsal region prior to surgery display large positive scores. The scores drop as one proceeds to the distal half of the flap in the measurements made after surgery. The difference in the reflectance of the distal section of the flap compared to the flap
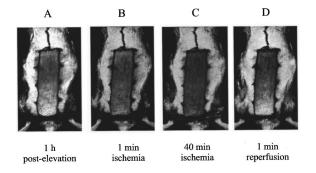
Fig. 7 Gray-scale first principal component score images of a flap derived from optical density near infrared multispectral images acquired 1 h after surgery (A), after 1 min (B), and 40 min (C) of skin flap ischemia, and 1 min after reperfusion (D).

Fig. 8 Mean ($\pm$SD) of 30 laser Doppler flux measurements of blood flow at each of the five measurement sites along the skin flap presented in Figure 7. Laser Doppler flux measurements were made immediately prior to surgery, 1 h after surgery, after 10 and 30 min of skin flap ischemia and 10 min after reperfusion.

base and surrounding uninvolved dorsal tissue dominates the variance in the logarithmic residual corrected postsurgery multispectral images. A comparison between the PC score images (Figure 6) and the laser Doppler measurements made on the same flap [Figure 1(B)] reveal a striking similarity in the response. Immediately following surgery the distal half of the flap shows a dramatic drop in perfusion and does not recover after surgery. The base of the flap displays an immediate drop in perfusion upon surgery but recovers over the next 12 h. The intermediate region, although less compromised than the distal half of the flap, shows no signs of recovery after surgery. This behavior correlates with the PC score image sequence in Figure 6 which in turn is consistent with the findings of Thorniley et al. during total occlusion of skin flaps and in the early reperfusion period.[1,4]

PCA was also carried out on visible-near infrared image sets. Generally, visible-near infrared multispectral images were found to be less sensitive to reflectance variations along the length of the skin flap compared to multispectral images based on near infrared wavelengths only.

Ischemia–reperfusion experiments were carried out on a series of three flaps. Vascular clamps, which were applied to the base of the flap, were used to totally occlude blood flow to and from the flap tissues. PCA analysis of the optical density and logarithmic residual corrected near infrared multispectral images was performed. Both preprocessing methods gave similar results. Figure 7(A) displays the first PC score image acquired 1 h following surgical elevation of the flap and immediately before vascular clamps were applied to the base of the flap. Consistent with all the other skin flaps studied, the 1 h postelevation score image displays a significant contrast between the base and the distal portion of the skin flap. Vascular clamping the base of the flap cuts off the blood supply to the entire flap. The laser Doppler measurements taken in parallel with the multispectral images (see Figure 8) indicate a significant drop in blood flow at sites 1, 2, and 3 once the clamps are applied to the base of the
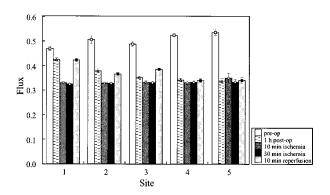
flap and there is an increased flow immediately upon release of the clamps. The score images acquired during vascular clamping [Figures 7(B) and 7(C)] show a uniform darkness (high negative score) over the full length of the flap. Immediately upon release of the clamps, a distinct gradient is observed to reappear between the base and distal sections of the skin flap in the score image [Figure 7(D)]. Similarly, the laser Doppler results reveal that blood flow in the base region of the flap undergoes an immediate hyperemic response upon release of the clamps which then approaches preclamping flow values within 10 min of reperfusion. Laser Doppler measurements at sites 4 and 5, which are situated on the distal half of the flap, show no response to clamping or reperfusion. Likewise, the distal section of the PC score images shows little change over the ischemia–reperfusion series of images, while the base shows a dramatic transition upon vascular clamping and the release of the clamps.

4 SUMMARY

This study uses the reverse McFarlane dorsal skin flap model in the rat to demonstrate the potential of multispectral imaging utilizing both visible- and near infrared wavelength measurement channels to detect poorly perfused tissues. By exploiting isobestic wavelengths and wavelengths at which Hb, HbO_2, and H_2O have significant differential absorptions, principal component image analysis of multispectral images can be used to assess tissue perfusion. Poorly perfused regions of flap tissue can be identified in the principal component score images taken immediately following surgery or in the early postoperative period, while overt clinical signs of compromised perfusion require 6–12 h to manifest. PCA as a multivariate technique does not explicitly monitor a single parameter. Rather it tends to group together correlated sources of variation and separate those sources of variation that are

not correlated. While this may initially lead to difficulties in the clinical interpretation of results, it may be that one or more PCs are a better correlate (predictor) with tissue viability than a single parameter (oxygenation, cytochrome aa3 redox state). This can only be determined after extensive experience and clinical testing of this approach. However, this paper demonstrates that PCA warrants further investigation as an analysis tool for multispectral images of skin flaps. The image processing methods presented in this paper are easily programmed and rapid in their execution. The acquisition and analysis of data can be easily performed within the surgical session and in the early postoperative period to provide the surgeon with immediate feedback regarding the perfusion status of the tissue being examined. Earlier detection of a perfusion related complication should enable prompt and more effective clinical intervention. We conclude that principal component analysis of multispectral near infrared images of skin flaps can potentially provide clinically relevant information on tissue perfusion in a manner that is both rapid and reliable.

Acknowledgments

REFERENCES

1. M. S. Irwin, M. S. Thorniley, C. J. Dore, and C. J. Green, ''Near infra-red spectroscopy: a non-invasive monitor of perfusion and oxygenation within the microcirculation of limbs and flaps,'' *Br. J. Plast. Surg.* **48**, 14–22 (1995).
2. R. E. Hayden, M. A. Tavill, S. Nioka, T. Kitai, and B. Chance, ''Oxygenation and blood volume changes in flaps according to near-infrared spectrophotometry,'' *Arch. Otolaryngol. Head Neck Surg.* **122**, 1347–1351 (1996).
3. M. S. Thorniley, S. Simpkin, N. J. Barnett, P. Wall, K. S. Khaw, C. B. Shurey, S. J. Sinclair, and C. J. Green, ''Applications of NIRS for measurements of tissue oxygenation and haemodynamics during surgery,'' *Adv. Exp. Med. Biol.* **411**, 481–493 (1997).
4. M. S. Thorniley, S. J. Sinclair, N. J. Barnett, C. B. Shurey, and C. J. Green, ''The use of near infrared spectroscopy for assessing flap viability during reconstructive surgery,'' *Br. J. Plast. Surg.* **51**, 218–226 (1998).
5. M. F. Stranc, M. G. Sowa, B. Abdulrauf, and H. H. Mantsch, ''Assessment of tissue viability using near infrared spectroscopy,'' *Br. J. Plast. Surg.* **51**, 210–217 (1998).
6. Y. Tosa, W. P. Lee, N. Kollias, M. A. Randolph, and J. W. May, Jr., ''Monoclonal antibody to intercellular adhesion molecule 1 protects skin flaps against ischemia–reperfusion injury: an experimental study in rats,'' *Plast. Reconstr. Surg.* **101**, 1586–1594 (1998).
7. Y. Tosa, N. Kollias, W. P. Lee, and J. W. May, Jr., ''Reduction of ischemia-reperfusion injury by monoclonal antibody to intercellular adhesion molecule-1,'' *Transplant. Proc.* **28**(3), 1210–1211 (1996).
8. B. M. Jones, R. Sanders, and R. M. Greenhalgh, ''Monitoring skin flaps by colour measurement,'' *Br. J. Plast. Surg.* **36**(1), 88–94 (1983).
9. M. G. Sowa, J. R. Payette, M. F. Stranc, B. Abdulrauf, M. D. Hewko, J. R. Mansfield, and H. H. Mantsch, ''Assessment of tissue viability by near-IR spectroscopy and imaging,'' *Proc. SPIE* **3257**, 199–207 (1998).
10. J. R. Payette, M. G. Sowa, S. L. Germscheid, M. F. Stranc, B. Abdulrauf, and H. H. Mantsch, ''Noninvasive diagnostics: predicting flap viability with near-IR spectroscopy and imaging,'' *Am. Clin. Lab.* **18**, 4–6 (1999).
11. M. G. Sowa, J. R. Payette, and H. H. Mantsch, ''Near infrared spectroscopic assessment of tissue hydration following surgery,'' *J. Surg. Res.* **86**, 62–69 (1999).
12. M. G. Sowa, J. R. Payette, M. D. Hewko, J. R. Mansfield, and H. H. Mantsch, ''Hemodynamic information obtained by statistical analysis of near-IR spectroscopic images,'' *Proc. SPIE* **3257**, 296–306 (1998).
13. J. R. Mansfield, M. G. Sowa, J. R. Payette, B. Abdulrauf, M. F. Stranc, and H. H. Mantsch, ''Tissue viability by multispectral near infrared imaging: a fuzzy *C*-means clustering analysis,'' *IEEE Trans. Med. Imaging* **17**, 1011–1018 (1998).
14. P. Geladi, H. Isaksson, L. Lindqvist, S. Wold, and K. Esbensen, ''Principal component analysis of multivariate images,'' *Chemom. Intell. Lab. Syst.* **5**, 209–220 (1989).
15. K. Okada, K. Segawa, and I. Hayashi, ''Removal of the vegetation effect from LANDSAT TM and GER imaging spectroradiometer data,'' *ISPRS J. Photogramm Remote Sens.* **48**, 16–27 (1993).
16. A. Singh and A. Harrison, ''Standardized principal components,'' *Int. J. Remote Sens.* **6**, 883–896 (1985).
17. R. M. McFarlane, G. DeYoung, and R. A. Henry, ''The design of a pedicle flap in the rat to study necrosis and its prevention,'' *Plast. Reconstr. Surg.* **35**, 177–182 (1965).
18. J. E. Jackson, *A Users Guide to Principal Components*, Wiley, New York (1991).
19. L. Cordone, A. Cupane, M. Leone, and E. Vitrano, ''Optical absorption spectra of deoxy- and oxyhemoglobin in the temperature range 300–20 K,'' *Biophys. Chem.* **24**, 259–275 (1986).
20. W. A. Eaton and J. Hofrichter, ''Optical spectroscopy of hemoglobin,'' in *Methods in Enzymology*, E. Antonini, L. Rossi-Bernardi, and E. Chiancone, Eds., Vol. 76, pp. 175–261, Academic Press, New York (1981).